Design and Modeling of a Force Sensitive Toothbrush by Using a Buckling Truss Structure

By

Jonathan Slocum

SUBMITTED TO THE DEPARTMENT OF MECHANICAL ENGINEERING IN PARTIAL FULLFILLMENT OF THE REQUIREMENTS FOR THE DEGREE OF

BACHELOR OF SCIENCE IN MECHANICAL ENGINEERING
AT THE
MASSACHUSETTS INSTITUTE OF TECHNOLOGY

June 2014

Signature redacted

Signature of Author: _____
Jonathan Thurston Slocum
Department of Mechanical Engineering
May 9th, 2014

Signature redacted

Certified by: _____
Ken Kamrin
Assistant Professor of Mechanical Engineering
Thesis Supervisor

Signature redacted

Accepted by: _____
Accepted by Annette Hosoi
Associate Professor of Mechanical Engineering
Undergraduate Officer

Design and Modeling of a Force Sensitive Toothbrush by Using a Buckling Truss Structure

By

Jonathan Slocum

Submitted to the Department of Mechanical Engineering
on May 9th, 2014 in Partial Fulfillment of the
Requirements for the Degree of Master of Science in
Mechanical Engineering

ABSTRACT

Excessive force applied to teeth with a toothbrush during brushing may cause tooth erosion and gum recession. There have been many attempts by others to mitigate this effect with a force-sensitive toothbrush that can alert a user when excessive force is applied. However, many of the prior art solutions to this problem do not have a tactile response to alert the user when excessive force is applied. Further many prior art solutions are often bulky, have multiple components, and/or are not aesthetically pleasing or ergonomic. Some prior art buckling structures also often had thin hinge sections which are difficult to injection mold and act as failure points and the resulting broken structure can be dangerous. Prior art buckling toothbrush structures further had the problem of once they buckled, the structure was so substantially weakened, that continued application of force could cause the structure to plastically fail.

A force-sensitive toothbrush incorporates a bistable truss into the neck of the toothbrush. The mechanism can alert a user to excessive brushing force by changing shape in response to brushing forces exceeding a predetermined threshold. The mechanism can also automatically return to its original state when the brushing forces are lowered back down below the predetermined level. The mechanism may include a force-sensitive region having an upper beam and a lower beam joined together to form a triangular truss, both grounded to the handle. This mechanism can advantageously be molded into an integral toothbrush body using an injection molding operation.

Thesis Supervisor: Ken Kamrin
Title: Associate Professor of Mechanical Engineering

Acknowledgements

The author would like to thank Professor Alexander Slocum for being a key partner in developing the toothbrush and force sensitive flexure every step of the way. He has made several key contributions to the design as well as been a major usability tester. One example of many is his contribution to the idea of modeling the toothbrush truss as a welded truss to predict internal forces and moments in the structure. This research could not have been done without his help.

Prof. Ken Kamrin also provided key insight on early iterations of the toothbrush design with regards to classifying buckling criterion as well as identifying how the structure was failing. Also Tomasz Wierzbicki provided other key insights to buckling modes of fixed-fixed geometries with multiple loading conditions.

Another major usability tester was Colleen Meehl, whose insight helped with defining future iterations of toothbrush flexures. Finally, Ken Stone and the MIT Hobby Shop for facilitating extensive Waterjet time and other tools for cutting testing flexures.

LIST OF FIGURES

Table of Contents

1. Introduction

Excessive force while brushing teeth can be detrimental to dental health. Toothbrushes are an essential part of dental hygiene and have been around for hundreds of years. Since its invention, the toothbrush has been redesigned many times and has evolved into a highly developed piece of engineering. Though they are critical to maintaining healthy dental hygiene, there have been several dental problems attributed to them. Overbrushing is the most common harmful side effect of using a toothbrush and can compromise dental health. Signs of these effects are receding gums, wearing of the enamel, and discoloration of teeth. A paper published in the Journal of Clinical Periodontology [1] showed that using for than 4 to 5N of brushing force had little effect removing more plaque. The study also concluded that only a few days were needed to show signs of gum damage.

Inventions developed from as early as 1984 [2] have tried to address the problem of brushing too hard with either force sensitive or pressure sensing toothbrushes. These devices alert users when they are brushing too hard on their teeth through either a tactile response or an electrical means like a light. The fundamental problem with these inventions is that they are either too complex, unwieldy, or have multiple parts. These attributes make them not viable to manufacture or pose a choking hazard to the user. A revolutionary force-sensitive toothbrush design was invented using a bistable flexure that buckles when the brushing force reaches a certain threshold. The toothbrush was designed with the functional requirement that it would alert users when they exert more than 5 ± 1N of force on their teeth and be able to manufacture the brush for under 5 cents

The design of this force sensitive toothbrush incorporates a bistable truss that buckles and creates a tactile feel for the user when they press too hard while brushing. The use of a buckling truss means that the structure will automatically restore itself if the user takes force off the brush, thus if they quickly apply too much force, the structure will simply fail again. The design and optimization of the truss is done by treating it as a welded structure. The addition of mesas to the toothbrush truss can help stiffen the brush for when users press too hard, thus protecting the structure from failure if a user is too rough with it. The use of a truss in a toothbrush to alert users when they are brushing too hard is a simple, yet effective method that barely changes manufacturing cost of the toothbrush.

2. Description of the Toothbrush Truss

A force sensitive toothbrush 1 is comprised of a triangular truss 3 that buckles when a threshold force is applied to the tip 11. The truss 3, shown in Figure 1 and Figure 2, is designed such that the lower member 7 elastically buckles to impact the small protrusion 5 on the brush side member 6 to create a tactile response for the user.

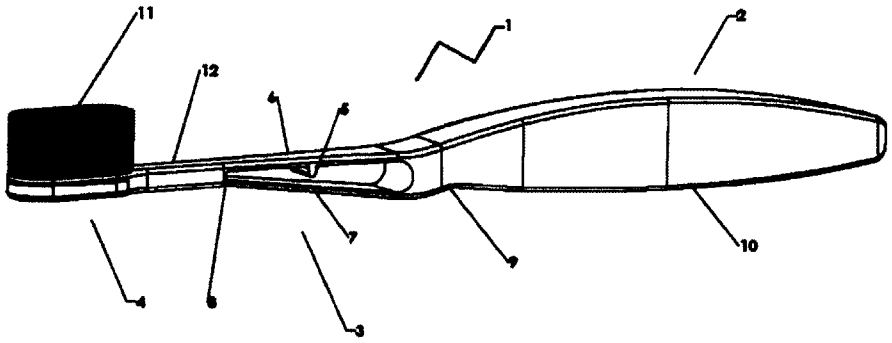

Figure 1: An isometric view of the toothbrush. The design shown here can be modeled as a simple triangular truss. The lower beam is designed to buckle upwards and create a snapping force.

Figure 2A shows a two dimensional view of the toothbrush and figure 2B shows a larger view of the flexure itself. Figure 2E and Figure 2F teach a notch 5a and key 5b configuration of the preferred embodiement, that when buckled, interlock to form a coherent structural loop between the brush side beam and the buckling-beam at the point of contact that stiffens the structure and reduces the chance of plastically yielding the buckled beam if the user continues to presses too hard. Figure 2F also teaches the same type of system where the orientation of the triangle with respect to the brush bristles has been flipped. This configuration is designed to work in the opposite direction to the flexure in Fig. 2B, thus the input force in this configuration is flipped to allow different styles of toothbrushes to be made with the same functionality.

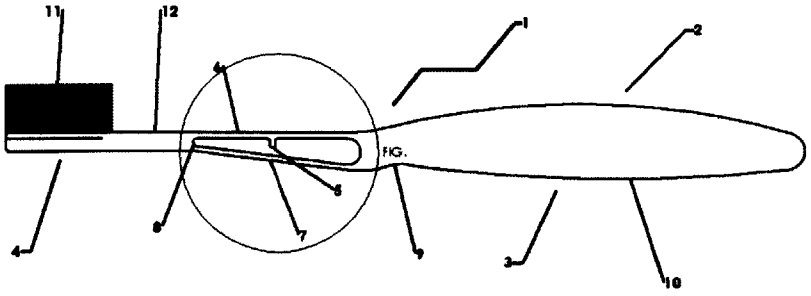

FIG. 2A

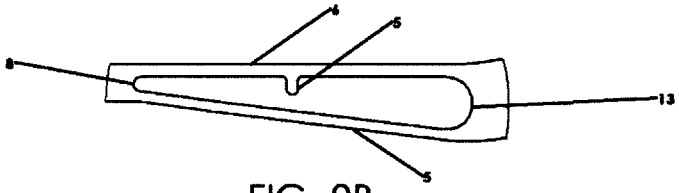

FIG. 2B

Figure 2A-2B: This is a full side view of an un-buckled toothbrush flexure with a single node. Also a close-up of the flexure with a single node

The toothbrush 1 includes a handle 2 and a force-sensitive truss region 3 that couples the head region 4 to a handle region 2. The handle 10 may have a suitable ergonomic grip, which features a thumb and forefinger placement area 9 for brushing bottom and top jaw teeth respectively. The flexure in figure 2B has a base region 13 of the triangular truss which marks the beginning of the flexure truss. The bristle-side beam 6 and the buckling-beam 7 meet together at the triangle vertex node 8. A stopper 5 is added to the bristle-side beam 6 to provide an anvil for the buckling-beam to snap against and create a tactile feeling when the buckling-beam 7 buckles inwards and strikes the stopper.

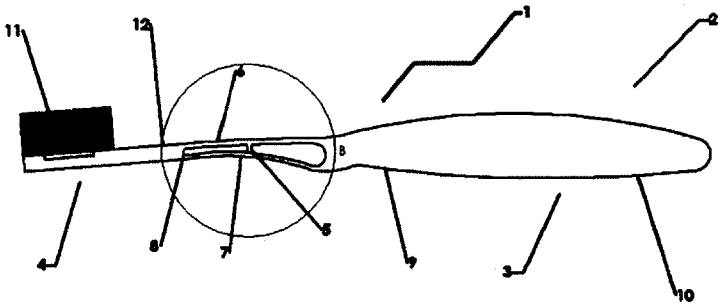

FIG. 2C

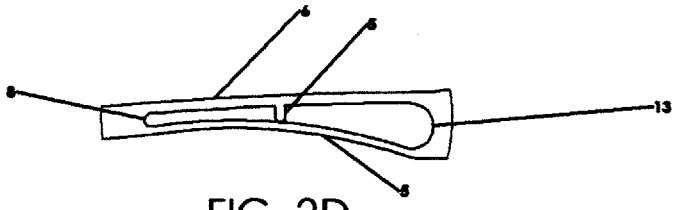

FIG. 2D

Figure 2C-2D: This is a full side view of a buckled toothbrush flexure with a single node. Also a close-up of the buckled flexure with a single node

A preferred embodiment stopper configuration shown in Figure 2E uses a notched (concave) mesa-like structure 5a and convex (key) mesa-like structure 5b configuration that creates the same tactile feeling, but the configuration is such that the structure will become more rigid and stronger when the buckling-beam elastically buckles as a result of the structural loop being completed by the notch and key structures engaging between the beams in their middle region when the buckling-beam has elastically buckled.

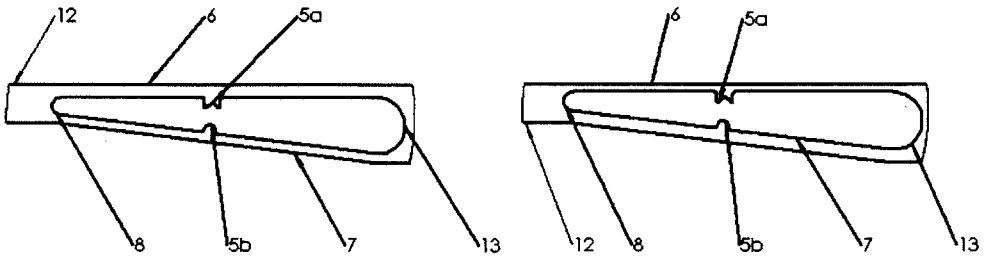

FIG. 2E FIG. 2F

Figure 2E-2F: A close-up of the toothbrush with an engaging notch. The theory is that the notch on the bristle side part of the brush 6 will engage with the node on the buckling beam 7, thus creating a stronger structural loop so the user won't permanently damage their toothbrush

The mechanical function of the notch and key is twofold: First for the brush-side-beam and buckling-beam between the engaged notch and key structures and the brush, it transmits shear forces between the beams which acts to stiffen them and act as a single thick beam region 18. This region is about half the length of the original truss members and now it also acts as a thicker beam and so is very strong.

Second, the engaged notch and key structures enable the creation of a temporary a second temporary truss like structure 17 whose base is the same as the original truss structure and whose vertex is at the engagement of the mesa-like structures. This smaller truss, with the same base dimension as the original, is very stiff and strong and prevents the elastically buckled buckling-beam from being overloaded and hence prevents the user from damaging the brush. The large increase in strength and stiffness prevents the elastically buckled buckling-beam from being further loaded to the point of plastic failure. This sudden increase in force, and indeed the transition from normal stiffness to sudden loss of stiffness, to sudden increase in stiffness is one more indicator to the user to back off on the brushing force. The effect is substantial and can help to prevent premature failure of the buckling-beam should the user ignore the pushing too hard sensation and continue to push hard on the brush.

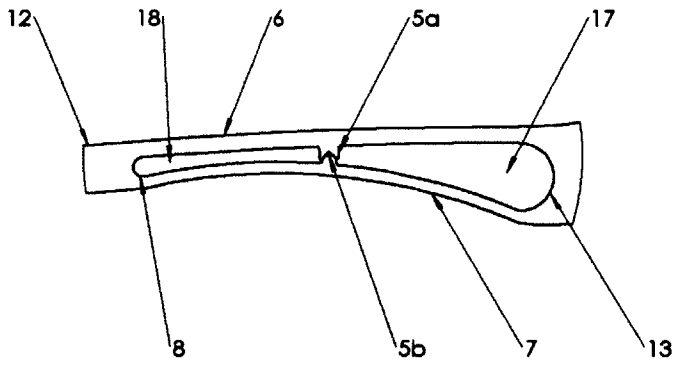

Fig. 2G

Figure 2G: This is a close-up of a bucked toothbrush truss with a notch and node configuration, thus completing the structural loop of the structure, making it stronger.

The preferred embodiment may also include a second set of notch and key mesa-like structures between the midspan mesa-like structures and the neck of the brush. These would also engage and act to even further stiffen and strengthen the beam region 18 when the buckling-beam has elastically buckled.

The neck 12 is joined with the node on one end and the head and the bristles 11 on the other. Figure 2C and 2D show the neck of the toothbrush after the structure has buckled. Note how the bottom beam has struck the stopper. This striking is what creates the defined clicking noise or tactile feeling to alert users that they are pushing too hard.

3. Modeling of the Toothbrush Truss

The truss in figure 3 schematically represents the truss of figure 2. An input force applied at the tip equates to a force F_{in} and a moment M_{in} at the point where the buckling-beam (lower member) 7 meets the brush-side-beam (upper member) 6 at the node 8. Since the toothbrush is a monolithic structure, the joints in the truss are considered to be "welded" for the sake of analysis.

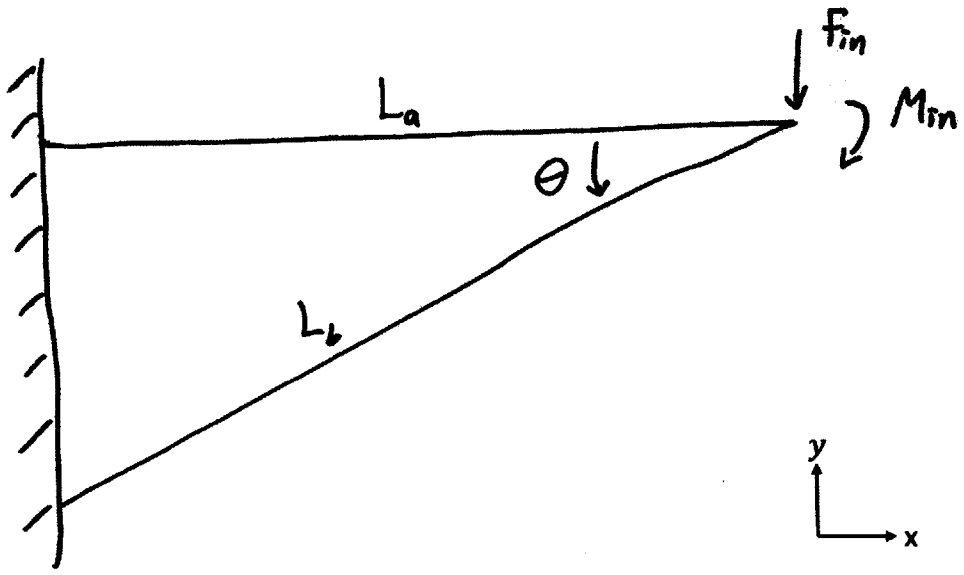

Figure 3: Simplified representation of the truss of Figure 2. It is important to note that the fixed end is where the handle of the brush lays, and the input force Fin is a result of the user and the internal moment M_{in} is a result of the user's force being applied over a given distance due to the bristles being apart from the flexure.

Figure 4 is a free body diagram of the individual links shown in figure 3. It shows the internal forces and moments the structure experiences at the node where the upper and lower members meet. By modeling the truss with the members having fixed end conditions a more easily manufactured design is obtained because hinge elements would require thin sections that are inherently more difficult to manufacture and likely to fatigue. As shown, there are six unknowns to be determined: four forces and two moments.

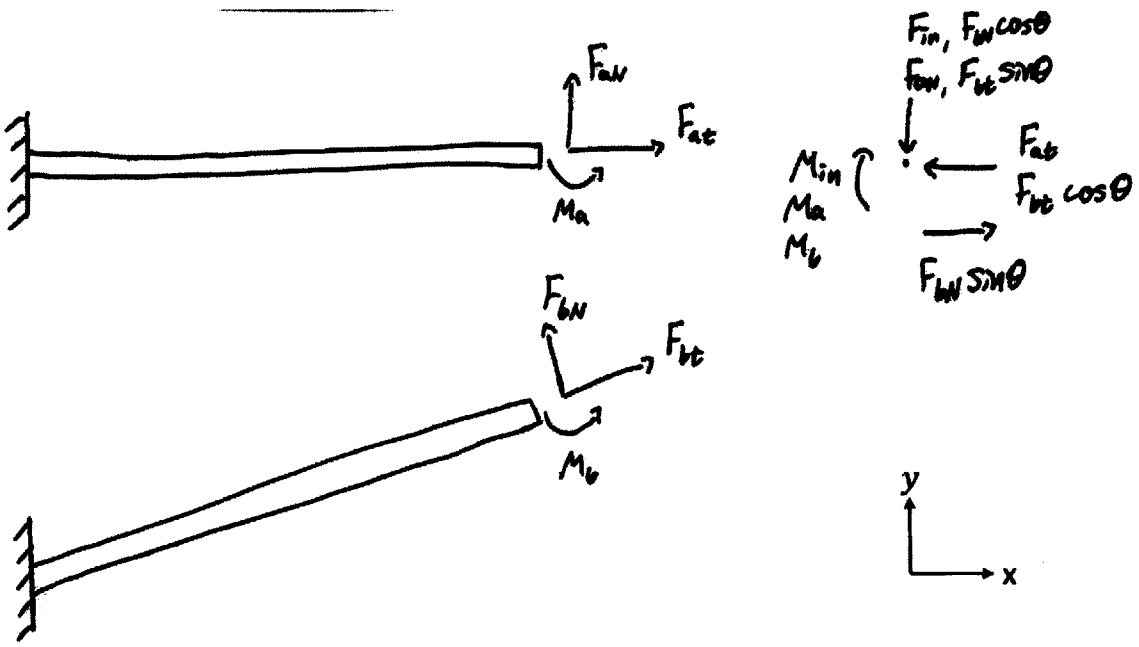

Figure 4: Free body diagram showing forces and moments experienced by each truss member where they meet at the node. The forces and moments in each beam are non-zero, thus neither member is a two-force member. These added forces and moments cannot be neglected since they play a key role in the buckling of the structure.

Summing the forces and moments at the node establishes the equilibrium equations for the node gives the following equations.

$$\sum F_x = F_{bN}sin\theta - F_{at} - F_{bt}cos\theta = 0 \tag{1}$$

$$\sum F_y = -F_{in} - F_{aN} - F_{bN}cos\theta - F_{bt}sin\theta = 0 \tag{2}$$

$$\sum M_z^{Node} = -M_{in} - M_a - M_b = 0 \tag{3}$$

Since the structure is statically indeterminate, there are more unknowns than there are equilibrium equations, geometric compatibility must also be considered. Geometric compatibility of the two beams at the node provides three additional equations. Since the upper and lower members are joined at the node, their deflections in both the x and y direction must be equal. Also their angular deflections (slopes) must be equal. Equations 4, 5, and 6 satisfy continuity at the node for each beam.

$$\delta_{xa} = \delta_{xb} \tag{4}$$

$$\delta_{ya} = \delta_{yb} \tag{5}$$

$$\emptyset_a = \emptyset_b \tag{6}$$

Since each member of the truss is a simple beam, these deflections can be determined with standard beam theory using the forces and moments shown in Figure 4 along with the material and geometric parameters of the members:

$$\frac{F_{at}L_a}{EA_a} = \frac{F_{bt}L_b cos\theta}{EA_b} - \frac{F_{bN}L_b^3 sin\theta}{3EI_b} - \frac{M_b L_b^2 sin\theta}{2EI_b} \tag{7}$$

$$\frac{F_{An}L_a^3}{3EI_a} + \frac{M_a L_a^2}{2EI_a} = \frac{F_{bt}L_b sin\theta}{EA_b} + \frac{F_{bN}L_b^3 cos\theta}{3EI_b} + \frac{M_b L_b^2 cos\theta}{2EI_b} \tag{8}$$

$$\frac{F_{aN}L_a^2}{2EI_a} + \frac{M_a L_a}{EI_a} = \frac{F_{bN}L_b^2}{2EI_b} + \frac{M_b L_b}{EI_b} \tag{9}$$

Thus there are obtained six equations with six unknowns, so the system can be solved. Equation 10 shows the system equations developed above in matrix form, which can then be solved closed form or numerically. Since their exact solutions are voluminous and very time consuming to manipulate, numerically solving the matrices is much more efficient. Table 1 also shows an example set of values used for a working flexure.

$$\begin{bmatrix} -1 & 0 & 0 & -cos\theta & sin\theta & 0 \\ 0 & -1 & 0 & -sin\theta & -cos\theta & 0 \\ 0 & 0 & -1 & 0 & 0 & -1 \\ \frac{L_a}{EA_a} & 0 & 0 & -\frac{L_b cos\theta}{EA_b} & \frac{L_b^3 sin\theta}{3EI_b} & \frac{L_b^2 sin\theta}{2EI_b} \\ 0 & \frac{L_a^3}{3EI_a} & \frac{L_a^2}{2EI_a} & -\frac{L_b sin\theta}{EA_b} & -\frac{L_b^3 cos\theta}{3EI_b} & -\frac{L_b^2 cos\theta}{2EI_b} \\ 0 & \frac{L_a^2}{2EI_a} & \frac{L_a}{EI_a} & 0 & -\frac{L_b^2}{2EI_b} & -\frac{L_b}{EI_b} \end{bmatrix} \begin{bmatrix} F_{at} \\ F_{aN} \\ M_a \\ F_{bt} \\ F_{bN} \\ M_b \end{bmatrix} + \begin{bmatrix} 0 \\ -F_{in} \\ -M_{in} \\ 0 \\ 0 \\ 0 \end{bmatrix} = 0 \tag{10}$$

L_a	40 mm
L_b	40 mm
t_a	1.667 mm
t_b	1.25 mm
m	25 mm
F_{in}	6.5 N
θ	7.125 deg.

Table 1 – These are used values for the analysis

Inputting the parameters shown in table 1 for the two beams with the moment arm, m (the distance the input force is from the node), yields equation 11.

$$\begin{bmatrix} F_{at} \\ F_{aN} \\ M_a \\ F_{bt} \\ F_{bN} \\ M_b \end{bmatrix} = \begin{bmatrix} -70.98\ N \\ -2.72\ N \\ 87.90\ Nm \\ 71.39\ N \\ -1.15\ N \\ 37.10\ Nm \end{bmatrix} \tag{11}$$

These results show that the dominant factors in the buckling of the buckling-beam are the axial forces (F_{at}, F_{aN}) and moments (M_a, M_b). The Normal (shear) forces experienced are relatively small, however they do still affect how the structure performs. To confirm these results are realistic, we consider a simple pinned truss with a single load applied at the tip as shown in Figure 5. By setting the input moment to zero in the code (M_{in}), Equation 10 yields the following results that are very close to those for a simple pinned joint truss.

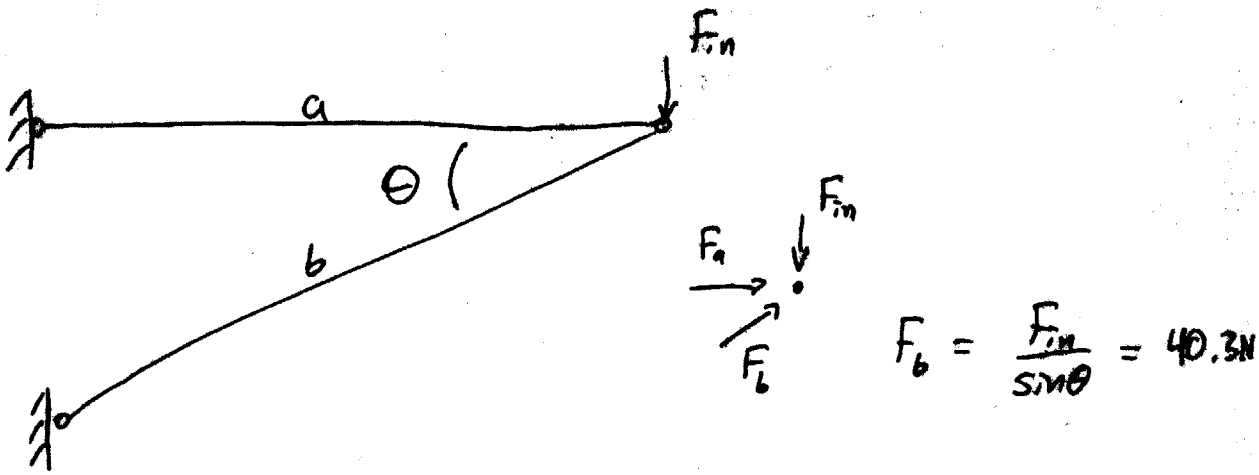

Figure 5: This shows a basic pinned truss under the same loading conditions. The axial force experienced by the buckling-beam is 40.3 Newtons, which is very close to the axial force experienced by the buckling-beam in Equation 12

$$\begin{bmatrix} F_{at} \\ F_{aN} \\ M_a \\ F_{bt} \\ F_{bN} \\ M_b \end{bmatrix} = \begin{bmatrix} -44.05\ N \\ -0.35\ N \\ 0.14\ Nm \\ 44.38\ N \\ -0.16\ N \\ 0.14\ Nm \end{bmatrix} \tag{12}$$

To gain insight on the model, Finite Element Analysis is also used. Figures 6 thru 11 show FEA models of the load (5N) placed at various distances from the node. As the force is applied further away from the node, the high stress areas move on the buckling-beam. This indicates that the moment generated by the input force begins to have larger effects as the force is moved away from the node.

To understand how to analyze the buckling criterion, it must first be understood that every force and moment acting on the buckling-beam will have some effect on the buckling criterion.

Experimentally a good snap was found when the force is applied at a distance of about 25mm from the node, as shown in Figure 11. The FEA shows a very even stress distribution in the buckling-beam as a result of the input. However as the distance is varied, the stress distribution becomes non-uniform. As the force approaches the node when the neck becomes short, the stress in the buckling-beam is due primarily to axial loading, however as the force moves away from the node, bending stress in the buckling-beam becomes more dominant. When this occurs, the beam is more reluctant to buckle outwards. At a certain distance, the moment is great enough to bias the buckling-beam to buckle inwards to always snap against the anvil, thus making it a successful design.

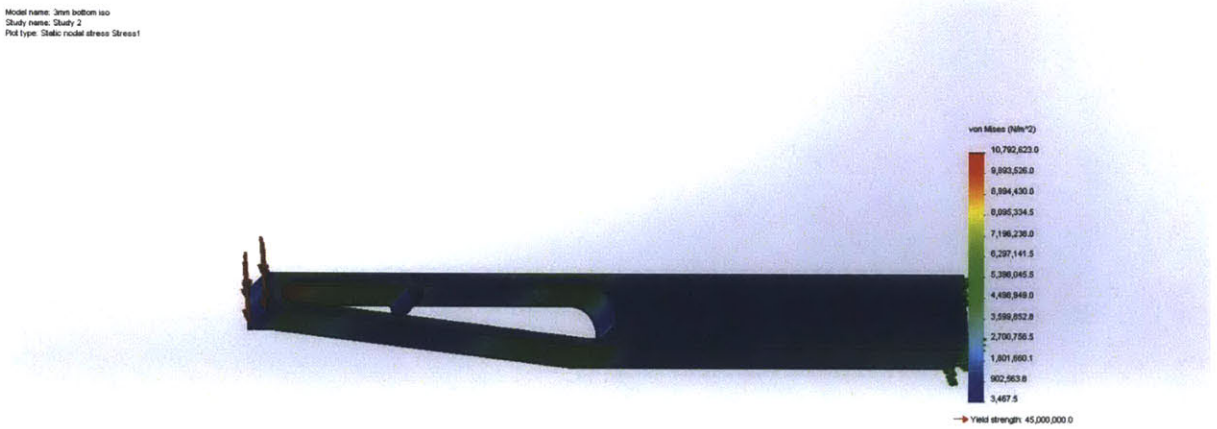

Figure 6: 5N load at 3mm from the node

Figure 7: 5N load at 10mm from the node

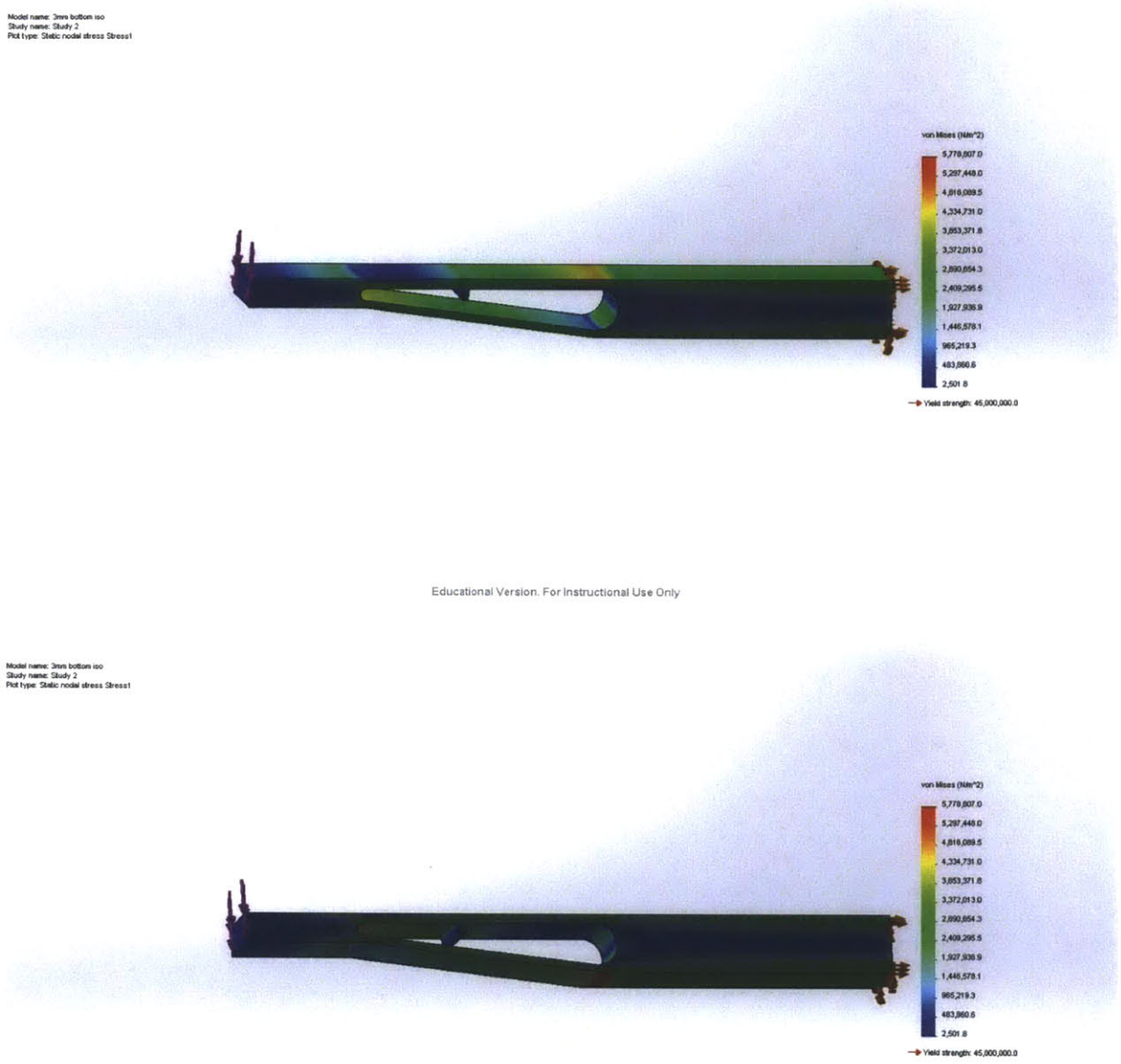

Figure 8: 5N load at 20mm from the node

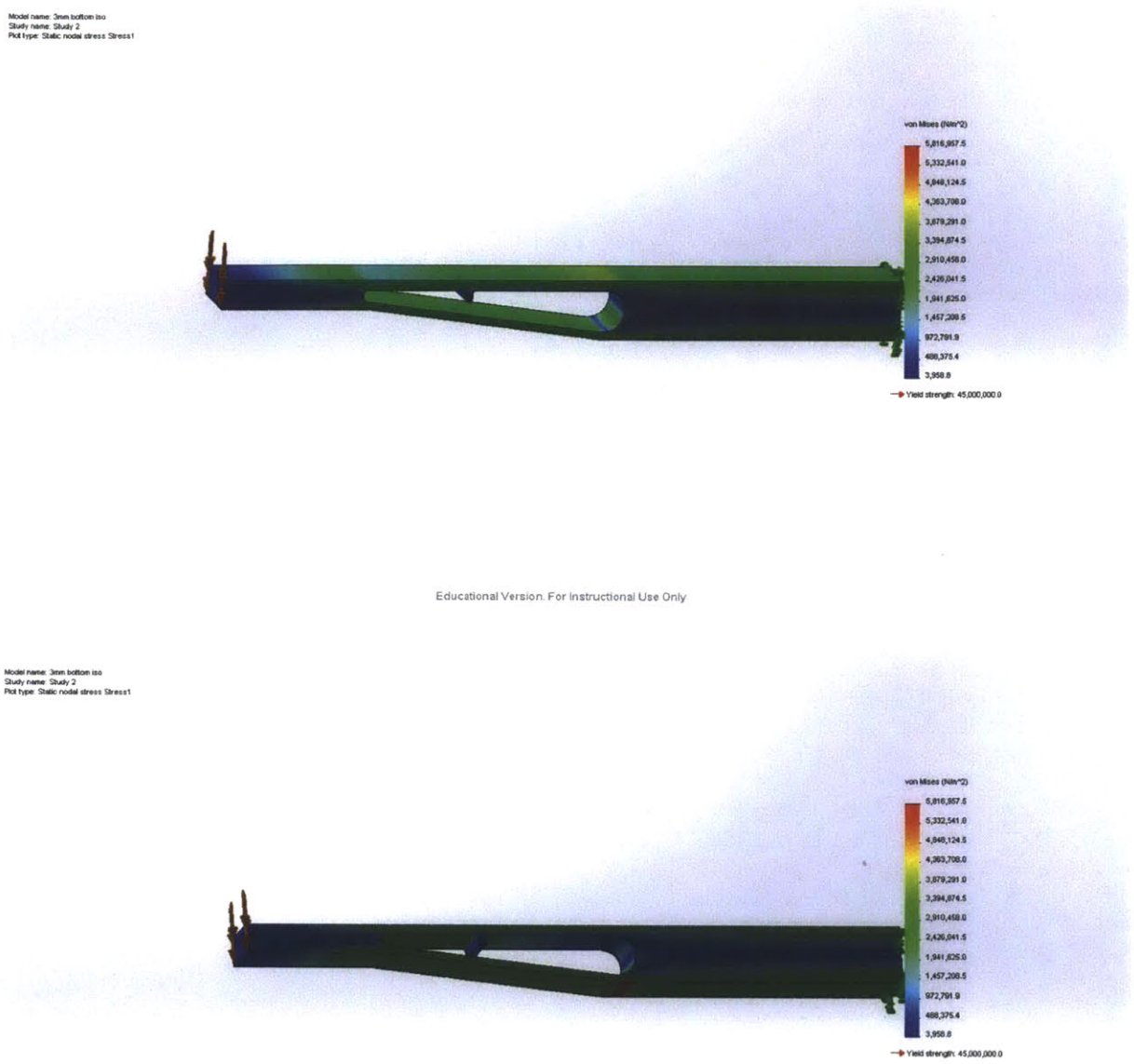

Figure 9: 5N load at 25mm from the node

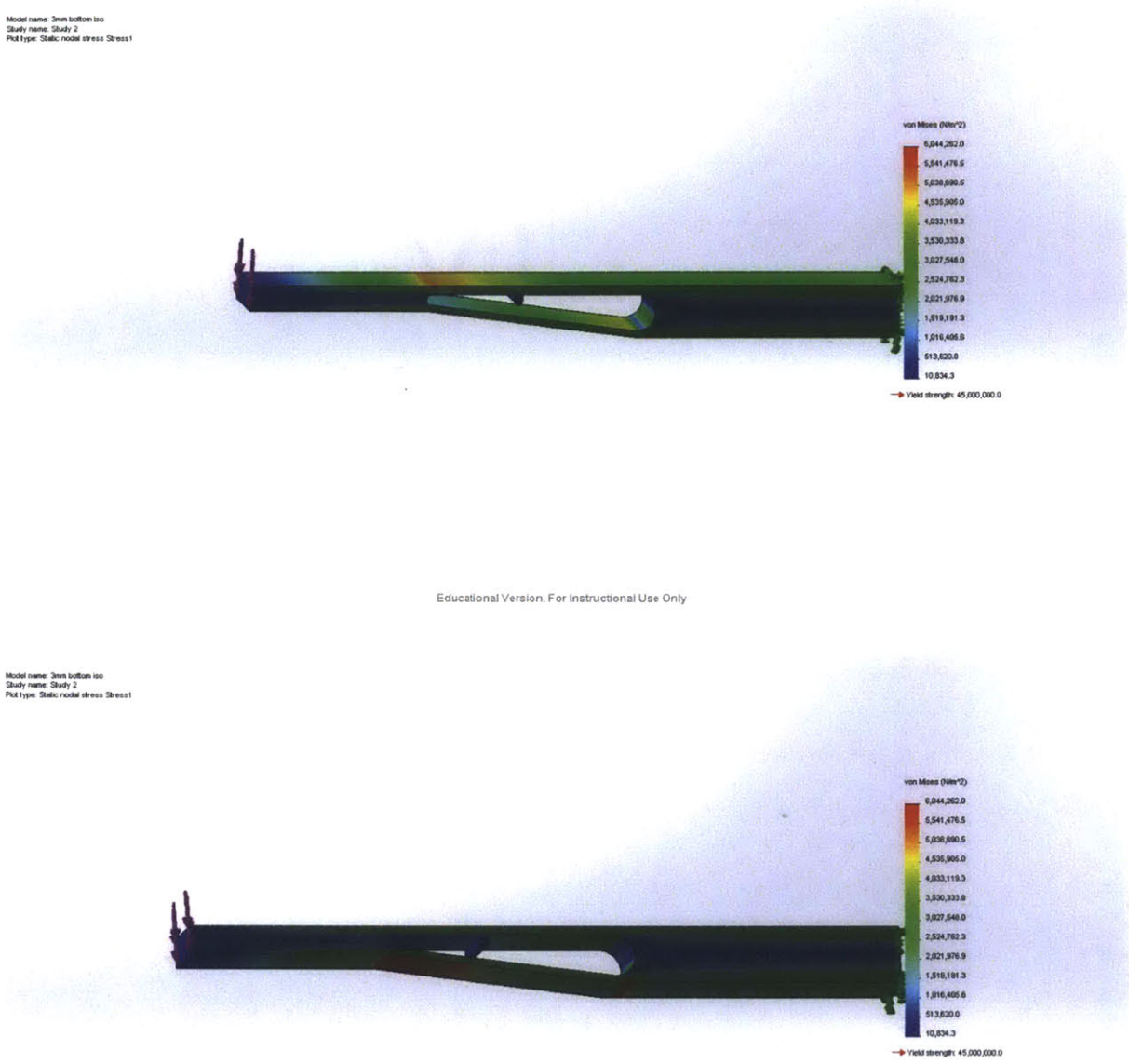

Figure 10: 5N load at 35mm from the node

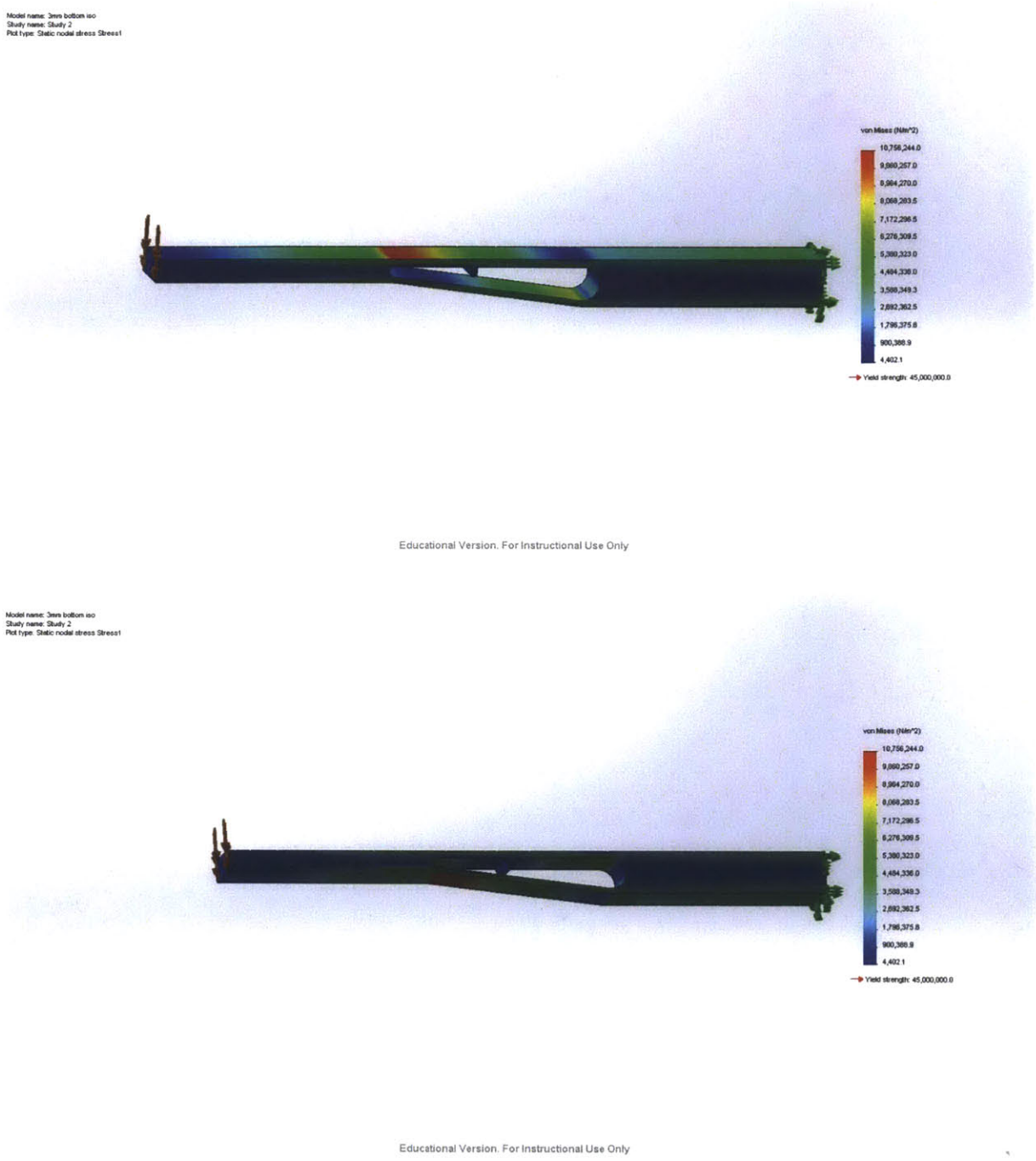

Figure 11: 5N load at 50mm from the node

Experimentally a good snap was found when the force is applied at a distance of about 25mm from the node, as shown in figure 11. The FEA shows a very even stress distribution in the lower beam as a result of the input. However as the distance is varied, the stress distribution becomes non-uniform. As the force approaches the node, the stress in the lower beam is due primarily to axial loading, however as the force moves away from the node, bending stress in the lower beam becomes more dominant. When this occurs, the beam is more reluctant to buckle

outwards. At a certain distance, the moment is great enough to bias the lower beam to buckle inwards, thus making it a successful design.

4. Buckling Criterion

When the buckling-beam is subjected to a high compressive stress, it will buckle, thus striking the bristle-side beam and causing a noticeable snap. The buckling of the bottom beam is a result of a compressive force, a normal force, and a moment applied to the beam. There is no single force or moment that is responsible for its failure, rather it is the combination that leads to the snap. In order for buckling to happen, a compressive stress threshold in the buckling-beam must be reached, and this compressive stress is due to the combination of the forces and moments on the beam.

This analysis approach for columns is presented in "Cold-Formed Steel Design" (Yu, Wei-wen, and Roger A. LaBoube. *Cold-formed Steel Design*. Hoboken, NJ: John Wiley & Sons, 2010), in which they describe a failure criterion as a result of a moment and an axial force applied to a single column. The total stress experienced in a column of length L and cross sectional area A is the sum of the axial stress and bending stress:

$$f = \frac{F_{bt}}{A_b} + \frac{M_b(t_b/2)}{I_b} \tag{13}$$

Where f is the total stress that the column experiences. For the toothbrush, a third bending stress term must be included as a result of the normal force and is shown in equation 14. The buckling threshold can thus be found in equation 15. This shows that the sum of the axial stress and bending stress in the beam must be less than the buckling stress in the beam in order for it to be stable. In equation 15, f_a represents the axial stresses and f_b represents the bending stresses inside the beam.

$$f = \frac{F_{bt}}{A_b} + \frac{M_b(t_b/2)}{I_b} + \frac{F_{bN}(t_b/2)(L_b - x)}{I_b} \tag{14}$$

$$f \geq f_a + f_b \tag{15}$$

So long as the total stress in the beam is less than a critical stress f, the buckling-beam will remain stable. Here, X is the distance from the base of buckling-beam b (7) to the node 8 where it joins with bristle-side beam a (6). Since the buckling-beam b experiences more than an axial force, the theory demonstrates that the maximum buckling load is a result of weakening in the beam due to the *parasitic* normal force F_{bN} and moment M_b. Figure 12 figuratively shows

how the stresses contribute to buckling. Note that the bending stress from the normal force is relatively low.

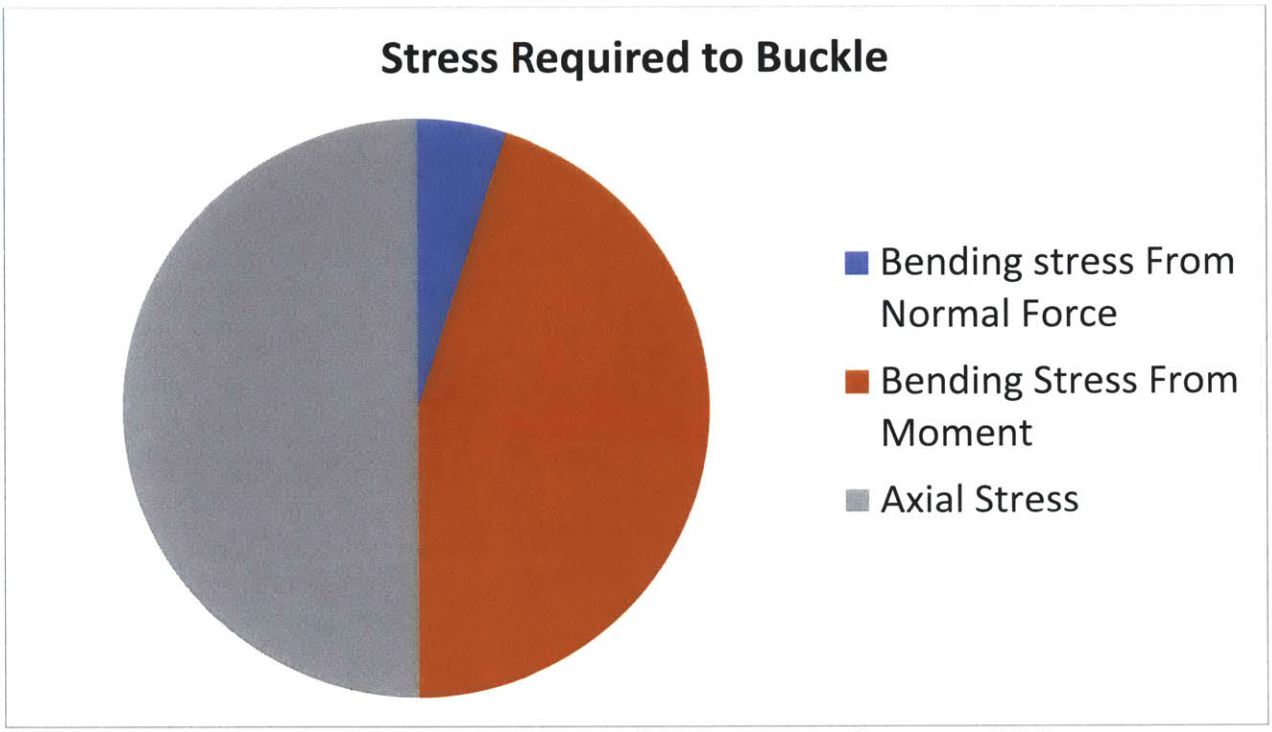

Figure 12: A pie chart showing the contribution of stress from an axial force, a normal force, and a moment experienced by the bottom beam.

Using this logic, a stress ratio can be derived from equation 15 in order to develop a buckling criterion. In order for the beam to buckle, no contributing stress can exceed its respective stress at failure. Equation 16 teaches that the ratio of the applied stress to the maximum stress before failure of each contribution must be less than 1 if the beam is to remain stable.

$$1.0 \geq \frac{f_a}{F_a} + \frac{f_b}{F_b} \tag{16}$$

Here, F_a is the maximum allowable axial stress and F_b is the maximum allowable bending stress. In F_b, both the moment and normal force contribute to the bending stress. This equation can also be rewritten as a ratio of forces and moments which is more useful in this case since the internal forces of the beam were solved for previously. Equation 17 shows the ratio of applied forces and moments to their respective maximum allowable forces and moments must be less than or equal to 1.0 in order for the beam to remain stable.

$$1.0 \geq \frac{F_{bt}}{F_{b\ Buckle}} + \frac{M_b}{M_{b\ yield}} + \frac{F_{bN}}{F_{bN\ yield}} \tag{17}$$

According to Yu and LaBoube, equation 17 (excluding the normal force term, $\frac{F_{bN}}{F_{bN\ yield}}$) is a well-known interaction formula used for short members and members subjected to a relatively small axial load. Since their analysis was used here for longer members with a more significant loading scheme, there is larger applied moment at mid span as a result of the beam having some curvature as a result of the initial applied moment. They assume there is an amplification factor φ which must be applied to the applied moment and normal force since the maximum moment occurs at midspan. Thus equation 18 shows the amplification factor and 19 is the buckling criterion to be used with the factor included.

$$\varphi = \frac{1}{1 - \frac{F_{bt}}{F_{b\ Buckle}}} \tag{18}$$

$$1.0 \geq \frac{F_{bt}}{F_{b\ Buckle}} + \frac{\varphi M_b}{M_{b\ yield}} + \frac{\varphi F_{bN}}{F_{bN\ yield}} \tag{19}$$

The maximum allowable forces and moments can be found using yield criterions and the general buckling equation. Using substitution, equation 20 shows the final buckling criterion equation for this analysis with the appropriate amplification factors. Table

$$1.0 \geq \frac{F_{bt}}{\left(\frac{EI_b\pi^2}{L_b^2}\right)} + \frac{\varphi M_b}{\left(\frac{\sigma_{yield} I_b}{(t_b/2)}\right)} + \frac{\varphi F_{bN}}{\left(\frac{\sigma_{yield} I_b}{(t_b/2)}\right)} \tag{20}$$

F_{bt}	Force along the longitudinal axis of buckling-beam
F_{bN}	Force perpendicular to buckling-beam at node
M_b	Internal moment in buckling-beam at mid span
φ	Correction factor
E	Modulus of elasticity
σ_{yield}	Yield stress of material
I_b	Area moment of inertia of buckling-beam

Table 2: This is a table of all the values used in the following buckling analysis

In order to check the validity of the above stability criterion, a measured result can be compared to a predicted result. A test was done on measured sample to determine what input force at a known distance would cause the structure to buckle in a preferred manner. Using a structure with a bottom beam equivalent thickness of 1.28mm and an bristle-side beam thickness of 1.50mm, it was determined the structure buckled favorably inwards (snapping into the stop) with 6.5 N of force with a minimum distance of 19mm from the node. Using equation 10 to solve for measured parameters, $F_{bt} = -80.42N$ for a 6.5N load.

To confirm the validity of the stability criterion in equation 20, F_{bt} can be solved for using the given parameters of the experiment and compared to the previously solved value. Equation 21 shows equation 20 rewritten solving for F_{bt}.

$$F_{bt} = \frac{EI\pi^2}{L^2}\left[1.0 - \left(\frac{\varphi M_b}{\left(\frac{\sigma_{yield} I_b}{(t_b/2)}\right)} + \frac{\varphi F_{bN}}{\left(\frac{\sigma_{yield} I_b}{(t_b/2)}\right)}\right)\right] \tag{21}$$

Using equation 21, with factor $\varphi = 1$, $F_{bt} = 58.03$ which is within 30% of the value obtained as a result of the experiment. Since this method is used in analysis aimed at preventing failure by buckling, it is expected that the predicted force required to buckle will be less than the actual force inside the beam. Nevertheless, it provides the designer with an analytical tool to design the truss so it can then be made, tested, and a final design more rapidly converged upon.

To further verify the stability criterion in equation 19, a second method from "Exact Solutions for Buckling of Structural Members" by C. M. Wang, C. Y. Wang, and J. N. Reddy (pgs. 9-14) can be used to calculate the critical axial force F_{bt} at buckling using Euler column buckling. Equation 22 shows the non-dimensional for Euler column buckling equation.

$$\frac{d^4w}{dx^4} + \alpha\frac{d^2w}{dx^2} = 0, \quad \alpha = \frac{F_{bt}L^2}{EI} \tag{22}$$

Here, w is the non-dimensional deflection, in which $w = \bar{w}/L$, $\bar{w}$ is the transverse displacement, and L is the length of the beam. Note that α contains F_{bt}. This equation has a general solution shown in equation 23 which can be further evaluated with various boundary conditions.

$$w = C_1 \sin\sqrt{\alpha}\, x + C_3 \cos\sqrt{\alpha}x + C_3 x + C_4 \tag{23}$$

Since the truss structure is not fully rigid, the bottom beam can be modeled as a column with elastic end restraints. Figure 13 is a figure from "Exact Solutions for Buckling of Structural Members" which depicts the buckling of a column with elastic end restraints.

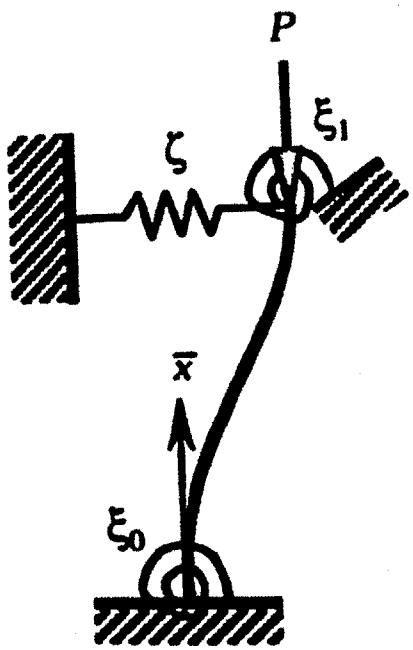

Figure 13: a buckled column with a rigid base coupled to an elastic foundation and two torsional springs at either end. The linear spring attached at the tip is meant to represent the fixed portion of the buckling beam to the brush-side beam (top beam).

Applying the appropriate boundary conditions and substituting in the non-dimensional spring constants ξ_0, ξ_1 and ζ, a general equation for the buckling criterion (equation 24) can be used for this particular case.

$$2 + \left[-1 + \left(\frac{1}{\xi_0} + \frac{1}{\xi_1}\right) + \alpha\left(\frac{1}{\xi_0\xi_1} - \frac{1}{\zeta} + \frac{1}{\xi_0\xi_1\zeta}\right)\right]\sqrt{\alpha}\sin\sqrt{\alpha}$$
$$- [2 + \alpha\left(\frac{1}{\xi_0} + \frac{1}{\xi_1}\right)\left(1 + \frac{\alpha}{\zeta}\right)\cos\sqrt{\alpha} = 0 \quad (23)$$

In the case of the truss structure, one end (the base) of the bottom beam is attached to the handle of the brush which deflects a negligable amount under the range of loading on the brush, thus it's treated as a rigid joint and the torsional spring ξ_0 will be assumed as having infinite stiffness. The bristle-side beam of the structure can be modeled as a linear spring that couples the buckling-beam at the node to a wall. In addition, the torsion spring at the tip of the beam ξ_1 correlates to the node where the two beams meet. This torsional resistance is a result of the moment created when the input force is placed at a known distance from the node. Equation 24 shows the relative stiffnesses of the linear and torsional springs.

$$K_{\xi_1} = \frac{3EI_a}{L_a^3}, \quad K_\zeta = \frac{EI_a}{L_a} \quad (24)$$

Using the conditions provided by Wang and Reddy in their book for columns with elastic end restraints, equation 25 gives insight on how to non-dimensionalize the stiffnesses so they can be used in equation 23. In order for these numbers to be non-dimensional, they must be normalized. Since these spring constants relate solely to the bristle-side beam, yet are coupled with the conditions in equation 24 which refer to the buckling-beam, they must be non-dimensionalized by the terms associated with the buckling-beam. As a result, equation 26 shows the final, non-dimensional spring constants coupled with the buckling-beam.

$$\xi_1\left[\frac{dw}{dx}\right]_{x=1}+\left[\frac{d^2w}{dx^2}\right]_{x=1}=0, \qquad \zeta w(1)+\left[\frac{d^3w}{dx^3}+\alpha\frac{dw}{dx}\right]_{x=1}=0 \tag{25}$$

$$\zeta=\frac{\left(\frac{3EI_a}{L_a^3}\right)}{\left(\frac{EI_b}{L_b^3}\right)}, \quad \xi_1=\frac{\left(\frac{EI_a}{L_a}\right)}{\left(\frac{EI_b}{L_b}\right)} \tag{26}$$

Using the assumption that the base of the buckling-beam is rigid ($\xi_0=\infty$), equation 27 becomes the final buckling criterion for the buckling-beam.

$$2+\left[-1+\left(\frac{1}{\xi_1}\right)+\alpha\left(-\frac{1}{\zeta}\right)\right]\sqrt{\alpha}\tan\sqrt{\alpha}-\left[2+\alpha\left(\frac{1}{\xi_1}\right)\left(1+\frac{\alpha}{\zeta}\right)\right]=0 \tag{27}$$

Since α contains F_{bt}, equation 27 can be solved for α, which has an infinite number of solutions because it involves an arctangent in the solution. These values, when matched to the data, come within 15-30% of the measured values, which is reasonable for buckling predictions, especially since they are conservative. Table 3 shows how different experiments varied as the buckling-beam thickness was changed from 1.25mm to 1.75mm while the bristle-side beam thickness stayed constant at 1.67mm. The measured buckling force in the buckling-beam is also compared to the predicted buckling forces and a percent difference calculated to show the percent difference.

Measured Buckling Force	Predicted Buckling Force Method 1	Predicted Buckling Force Method 2	t_a/t_b	Percent Difference Method 1	Percent Difference Method 2
83 N	57.8 N	60.14 N	1.28	% 30.36145	% 27.54217
98.61 N	69.99 N	75.56 N	1.19	% 29.02343	% 23.37491
120.36 N	87.17 N	98.74 N	1.09	% 27.57561	% 17.96278
153.28 N	95.77 N	117.28 N	1.02	% 37.51957	% 23.48643
154.69 N	106.65 N	130.18 N	0.99	% 31.05566	% 15.84459

Table 3: This shows how the buckling force of both predicted and measured values compared as the thickness ratio of the buckling beam and the brush side beam varied.

Figure 14 shows a graph of measured and predicted results for 5 different toothbrushes with triangular truss force sensing regions. A force sensor was placed at 20mm from the node to measure the buckling force for every truss. The thicknesses of each truss were also measured. Using these parameters, the internal force was determined at the point of buckling for each brush. These forces were then compared to forces each buckling criterion yielded and plotted as a function of the bristle-side beam thickness to the buckling-beam thickness. The results show that the second buckling prediction method follows a similar trend line to the measured results.

Predicted Buckling Force vs. Measured Force of lower beam at 20mm from Node

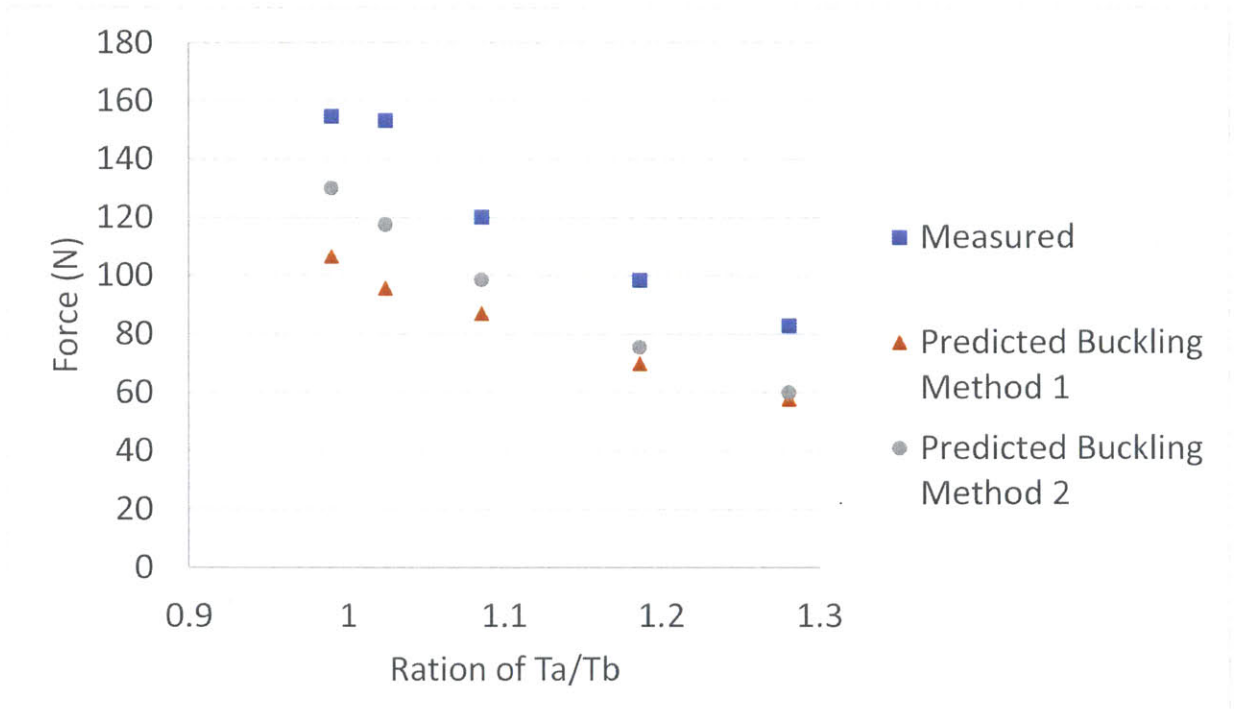

Figure 14: This is a graph showing the predicted buckling force vs. the measured buckling force of the lower beam at 20mm from the node. Both buckling theories are compared here. Method 1 is using simple fixed-fixed approximations and Method 2 is using the unique solution method

The ability to use closed-form analysis to create the basic design of the truss is very important to allow the user to rapidly converge on a design, and indeed do parametric studies including the effect of manufacturing tolerances on performance. Once the design is created, finite element methods can be used to check the design; however it should be noted that at this point a real prototype can also be easily be made and tested.

Figures 14 thru 18 show a variance of difference surface plots that change according to upper and buckling-beam thicknesses. The horizontal plane shows the zero plane for reference. The figures plot stress of the bottom most fibers of the buckling-beam as a function of the length of the buckling-beam and the distance over which the input force is applied. These figures illustrate a threshold for buckling. So long as there is a compressive stress in the bottom fibers of the buckling-beam, the buckling-beam will favor a concave shape, thus theoretically it will always buckle into the bristle-side beam so long as parameters are selected below the plane at

zero stress. However, from testing and experiments, the brush truss tends to take an unpredictable shape when the force is applied closer than about 20mm to the node. This may be due to how the force is applied and the extent of manufacturing tolerances.

Further modifications of the invention will also occur to persons skilled in the art, and all such are deemed to fall within the spirit and scope of the invention as defined by the appended claims.

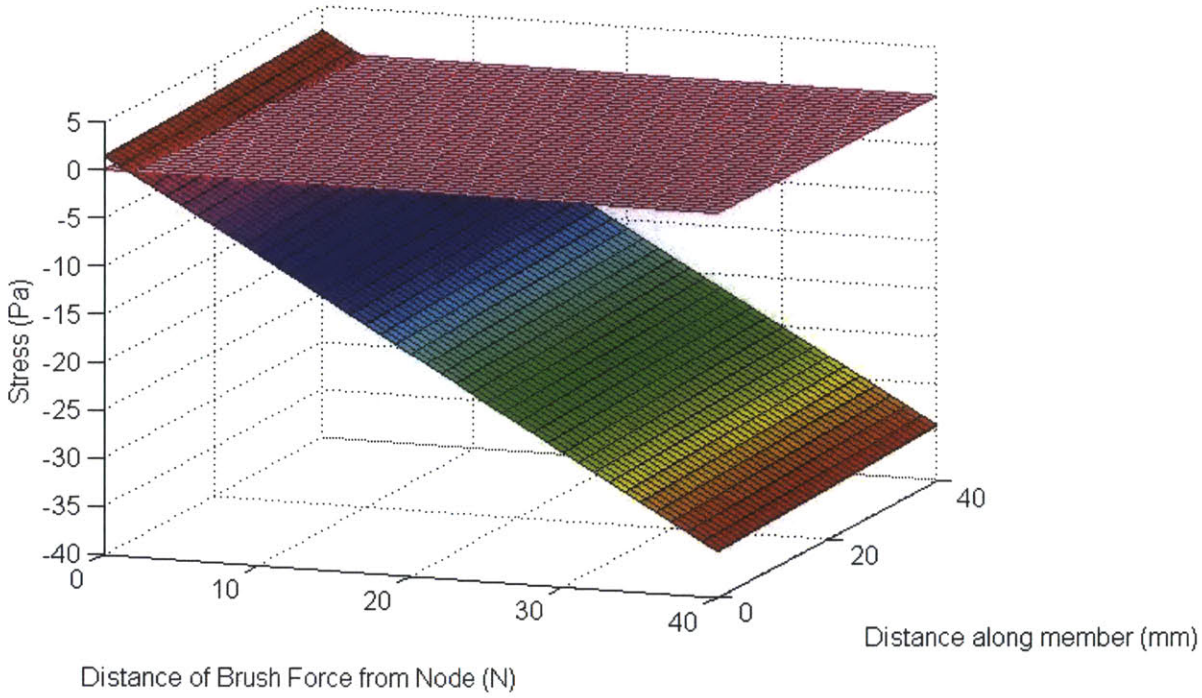

Figure 15: This is a surface plot of the stress (z axis) vs. the length of the buckling-beam in Fig 2B and distance over which the input force is applied. This plot has a top beam thickness of 1.67 mm and a bottom beam thickness of 1.25 mm. The red plane represents a plane at zero stress, thus any positive stress represents an unstable region. This gives a criterion for designers to select a distance at which the truss must be from the brush to the first node of the truss

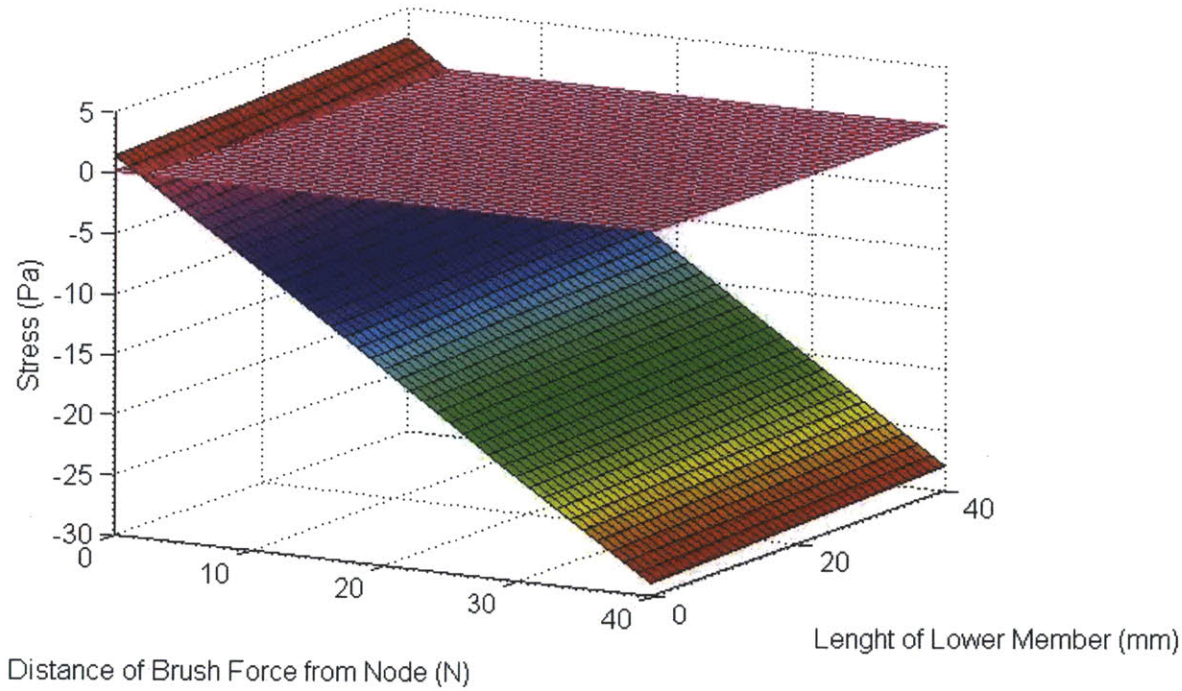

Figure 16: This is a surface plot of the stress (z axis) vs. the length of the buckling-beam in Fig 2B and distance over which the input force is applied. This plot has a top beam thickness of 1.67 mm and a bottom beam thickness of 1.38 mm. The red plane represents a plane at zero stress, thus any positive stress represents an unstable region. This gives a criterion for designers to select a distance at which the truss must be from the brush to the first node of the truss

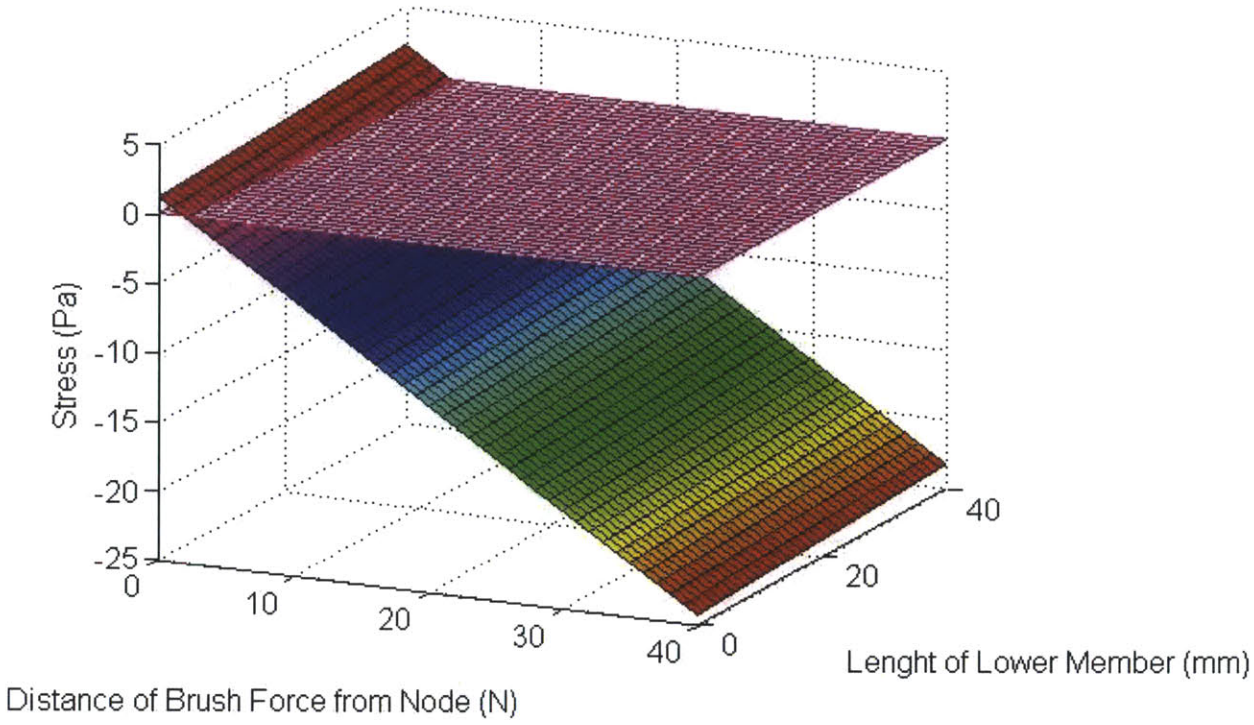

Figure 17: This is a surface plot of the stress (z axis) vs. the length of the buckling-beam in Fig 2B and distance over which the input force is applied. This plot has a top beam thickness of 1.50mm and a bottom beam thickness of 1.38 mm. The red plane represents a plane at zero stress, thus any positive stress represents an unstable region. This gives a criterion for designers to select a distance at which the truss must be from the brush to the first node of the truss

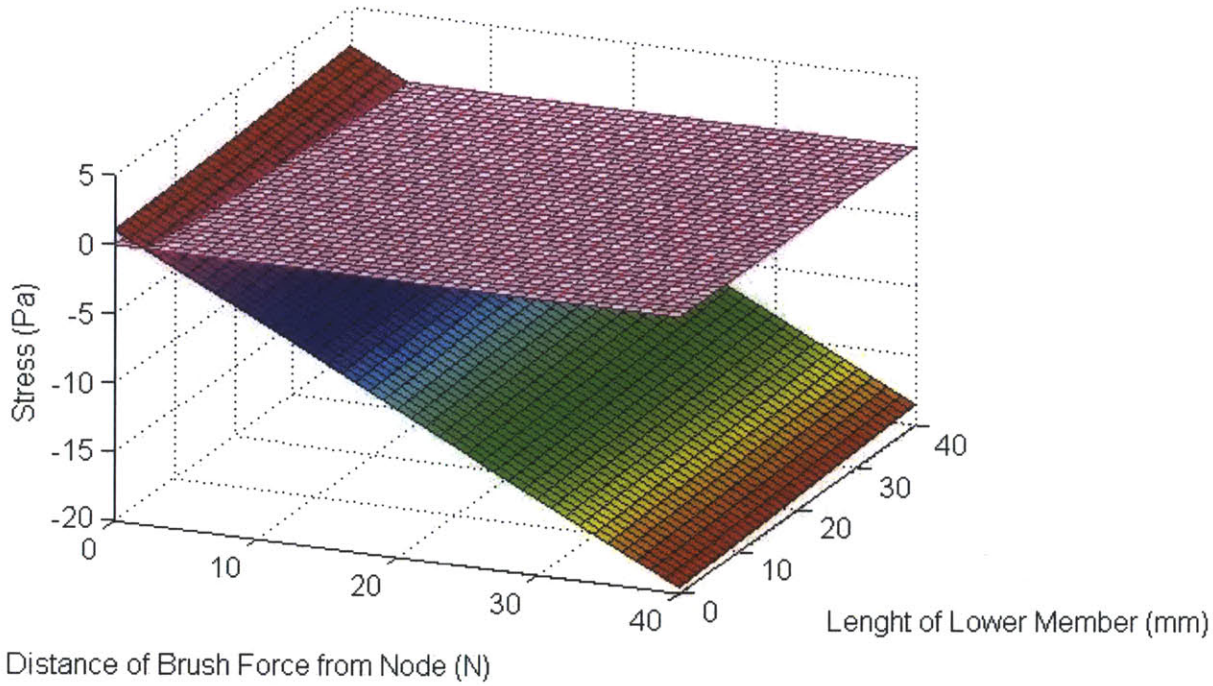

Figure 18: This is a surface plot of the stress (z axis) vs. the length of the buckling-beam in Fig 2B and distance over which the input force is applied. This plot has a top beam thickness of 1.67 mm and a bottom beam thickness of 1.67 mm. The red plane represents a plane at zero stress, thus any positive stress represents an unstable region. This gives a criterion for designers to select a distance at which the truss must be from the brush to the first node of the truss

5. Multiple Mesas

An Experiment was done to test the effects of different types of stoppers. Ideally, a user will brush until the structure buckles. However, in the event that a user continues to brush and with more force, the structure could become compromised. After the buckling side beam has collapsed, it generates two separate structural loops as shown in figure 19. These loops both act as truss shapes of their own with finite buckling loads as well, thus when a user presses much harder than the designed force, each of these loops will fail in second and third order buckling modes.

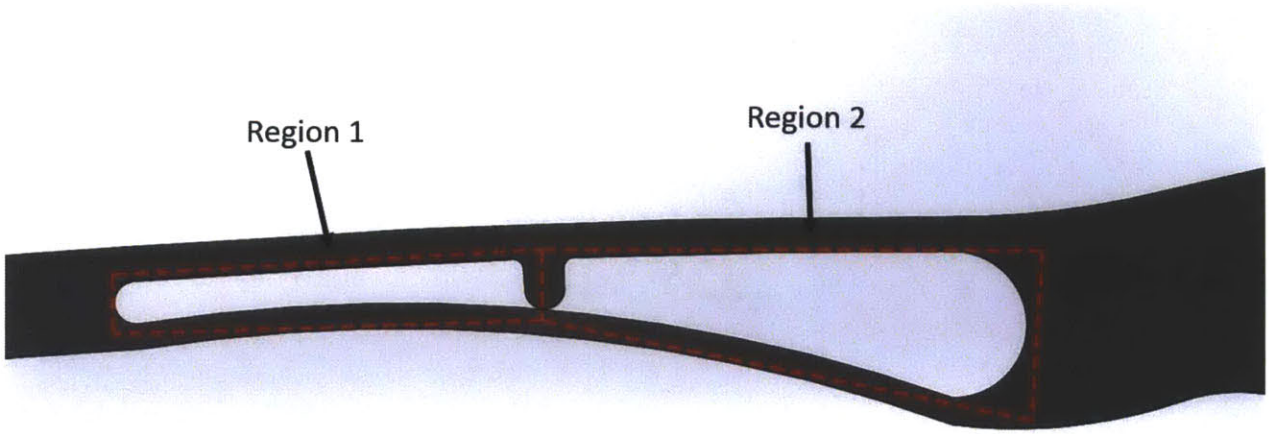

Figure 19: This is shows how there are two separate, smaller structural loops created when the node strikes the buckling beam. Thus these regions have their own bucking modes. Region 2 experienced the first mode since it has a longer member present

Since the internal moment of the buckling beam increases away from the brush head, region 2 is most susceptible to buckling because it's closest to the fixed end. Thus it was thought some slip was occurring at the single node shown in figure 20 that was helping this to happen. As a result, a locking mesa was added instead of a single node so that no slip would occur as shown in figure 20. This locking mesa acts as a pivot for both regions, thus allowing both regions to react like pinned trusses when subjected to excessive loads.

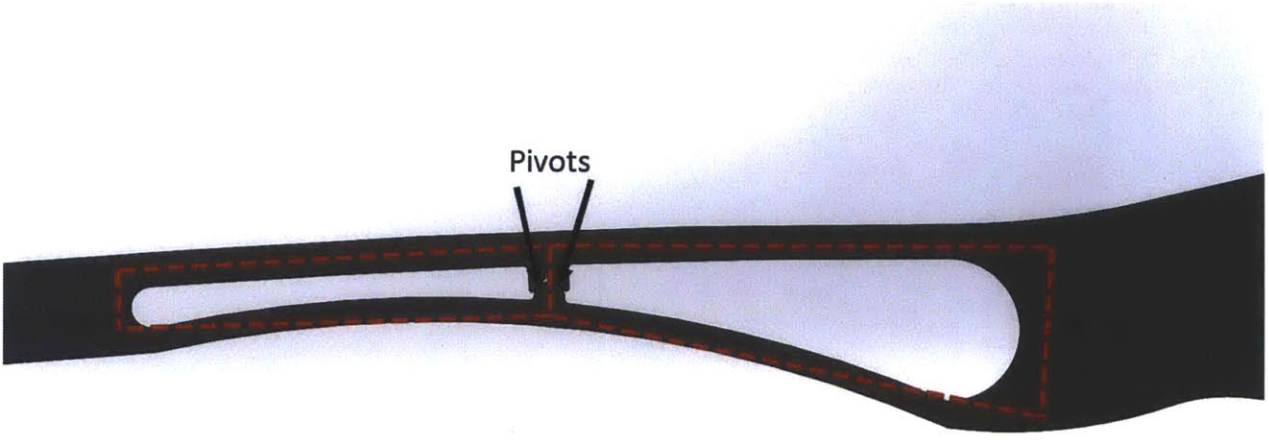

Figure 20: The pivot forms as a result of the first mesa forming, thus creating another truss like structure in both regions, shown in figure 19.

This single mesa is not enough to counter the buckling, thus a second mesa was added to counter the second buckling mode, thus creating a third structural loop that will help prevent the brush.

This second mesa is shown in Figure 21. The second mesa is placed in the second region to counter buckling of the newly formed member when the first mesa forms.

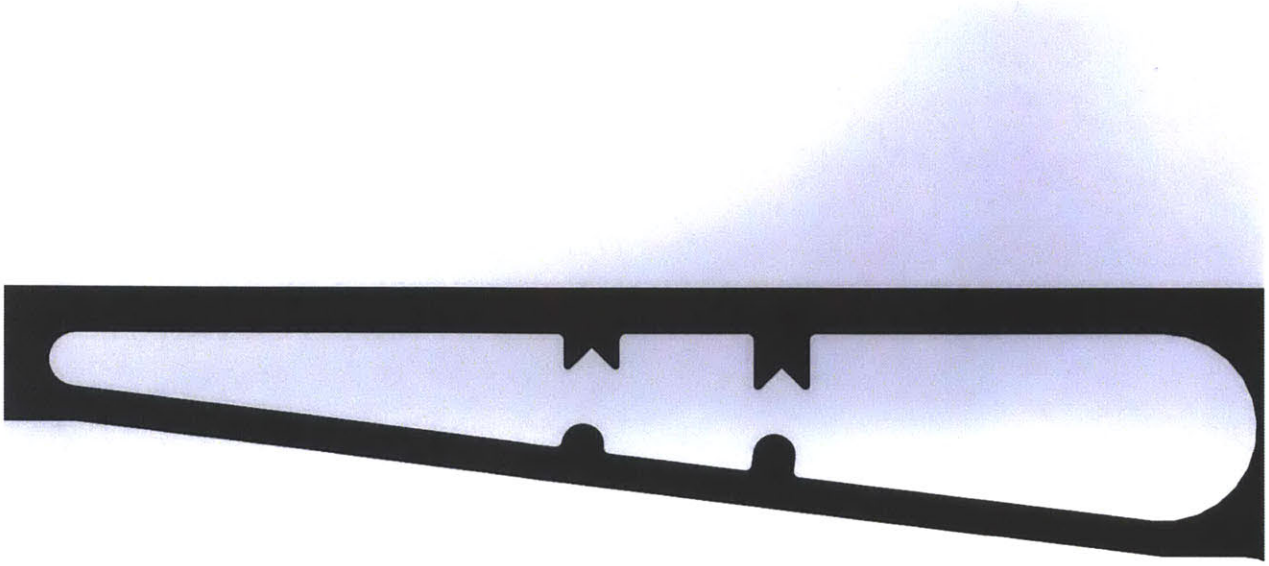

Figure 21: This shows the second mesa in the toothbrush truss. The second mesa helps counter the second buckling mode that occurs after the first mesa forms, as a result it stiffens the structure significantly.

Test data was also collected to show the significance of adding a second mesa to the structure, compared to a single node and a single mesa. Figure 22 shows a graph that was obtained by measuring the force applied to the structure as a function of the deflection of the structure.

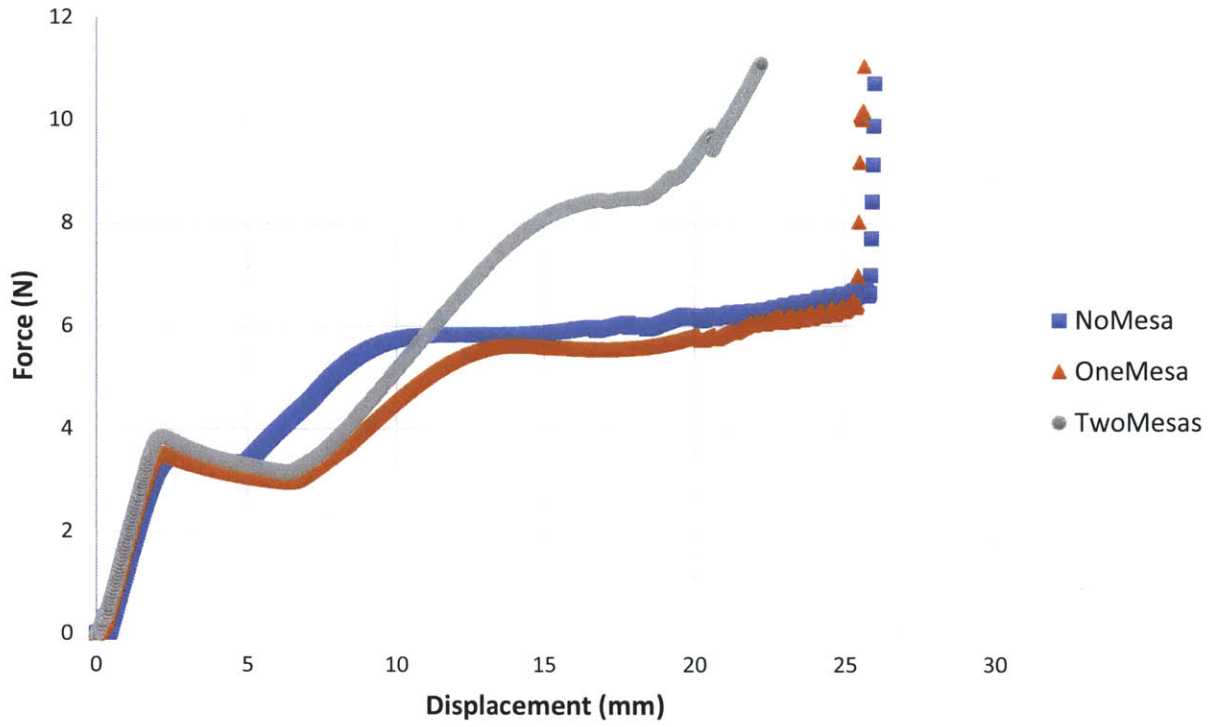

Figure 22: This shows the force applied to each type of truss described as a function of the displacement at the tip of the structure. As shown, the structures act similar until about 2mm of displacement occurs, at which point they all act differently. The most important part to note is the stiffness generated by two mesas. Both structures with no mesa or a single mesa experience buckling at about 10mm, as shown by the constant force.

This graph shows that adding a second mesa stiffens the structure significantly. As a result, if a user were to crash the brush, abuse it in some way it was not intended, or is just a hard brusher that does not want to heed the warning of the device, the second mesa would help strengthen the structure and help prevent permanent damage to the structure.

6. Fatigue Testing

Fatigue testing was done using a motor to determine how long the structure would last before the brush user would have to buy a new brush. Figure 23 shows a cam design used to buckle the truss repeatedly until failure occurs. It is estimated that a user would go through at most 50 cycles of buckling initially during each brushing routine. Toothbrushes, as recommended by dentists, should be changed out for new ones every 3-6 months, however it should be assumed for design considerations that people don't get new toothbrushes until they visit the dentist next, which is generally every year.

Figure 23: This is a fatigue testing using a cam that rotates between 1 and 2 Hz. Each cycle fully buckles the toothbrush truss. This simulates a user buckling the structure while brushing.

Samples were taken at controlled intervals and plotted. The results are shown in figure 24. The force required to buckle the structure compared to the number of cycles that had passed gave valuable insight on how the structure performed as a whole since fatigue cracking was an issue. This is probably because the flexure was water jetted and micro cracks in the structures surface helped facilitate small fatigue cracks. The structure was buckled 90 times a minute, so thermal effects may have also been an issue, but the structure lasted for thousands of cycles, which when extrapolated to a real situation, the user could use the same brush for several months without seeing any change in performance of their toothbrush.

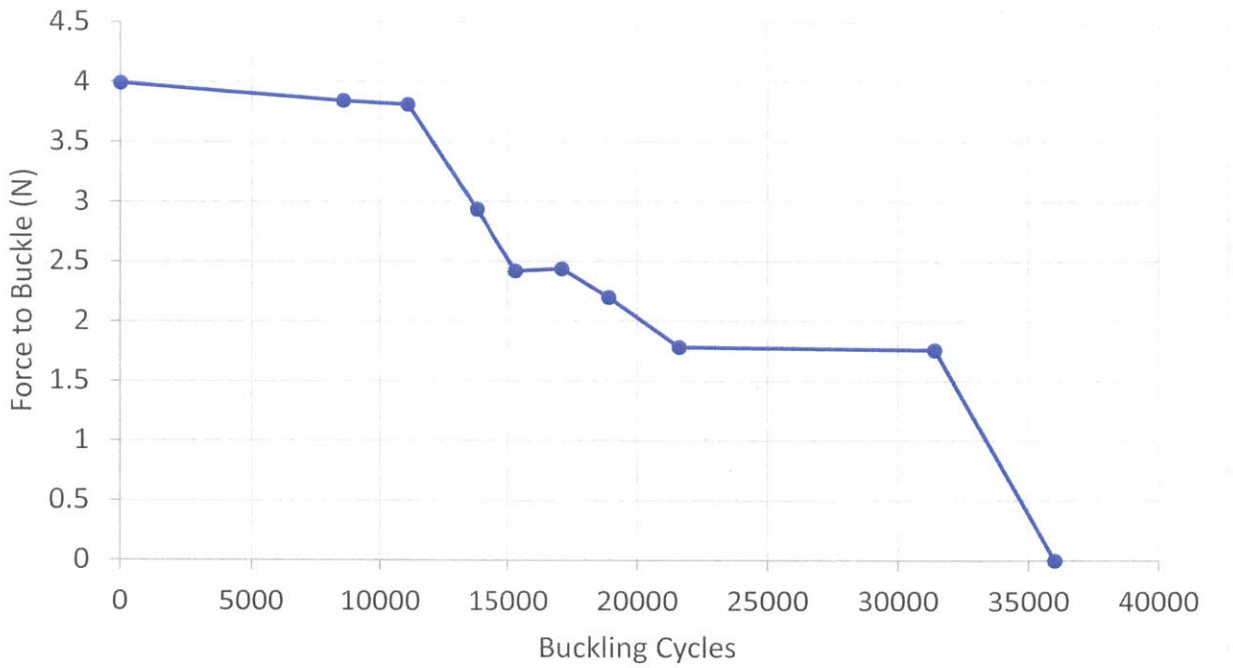

Figure 24: This is a graph showing the fatigue testing done on the toothbrush truss with a single mesa. After about 12000 cycles there is a significant drop in performance of the structure. However, would be well after a year's worth of use on the structure.

The fatigue data shows that the toothbrush structure lasted until about 12000 cycles. However, this was done at 1.5 Hz. The toothbrush structure showed micro-cracks at sharp corners and where the mesas were placed, indicating that there were significant stress concentrations. Also the structure was slightly warm immediately after the testing was stopped, thus the structure may have been tested at too high a sample rate that it interfered with the fatigue testing. Assuming a brush user will not exceed 10 cycles per brushing period after they have learned to use the toothbrush, this structure can last more than a year without a major change in performance.

7. Conclusions

As there are major dental problems associated with using excessive force while brushing, a device that tells the user when they are brushing too hard is needed, as suggestions by dentists is clearly not enough. The use of a buckling truss on a toothbrush is a direct method of informing a user when they are brushing too hard, however if the user wants to ignore the system, they can simply do so and continue brushing without any interference from the truss.

Since the design of the brush must be robust, mesas may be added to help stiffen the brush. Multiple mesas allow for the brush to stiffen once the buckling beam has struck the top beam and alerted the user they are brushing too hard. One issue that does arise is the problem of pinching tissue if the flexure is in a user's mouth while they brush. This can be avoided by narrowing the lower beam so it is not flush on the sides with the brush side beam, however further research is needed. Also other mesa like structures can be explored to further enhance stiffening the brush and make possible injection molding optimization more simple. Finally, the use of chemicals by users may also have an odd effect on the overall performance. Some users soak their toothbrushes in mouthwash to keep them germ free. This might have some effect on the plastic used for the truss if left in for long periods of time.

Since the brush does not take up considerably more plastic, it is possible that it will not change the price of manufacturing by more than 5 cents as previously states. Finally, the force threshold of truss structures that are sized for toothbrushes are between 2N to 5N which is right in the optimal threshold requirement. More work must be done to integrate the truss into an actual working toothbrush which can then be injection molded, impregnated with bristles, and given to a user. Thus this product has viability, but further testing and design must be done before it can be brought to market as other iterations must be done.

References

1. G. A. Van der Weijden, M. F. timmerman, M. M. Danser, and U. Van der Velden, "Relationship between the plaque removal efficacy of a manual toothbrush and brushing force", Journal of Clinical Periodontology, The Netherlands, 1998 (Published)

2. L. W. White and L. Ingles, "US Patent 4,476,604 Pressure Sensing Device For Holding a Toothbrush", United States Patent Office, Washington DC, Oct. 16 1984 (Patented)

3. G. A. Van der Weijden, M. F. timmerman, M. M. Danser, and U. Van der Velden, "High and low brushing force in relation to efficacy and gingival abrasion", Journal of Clinical Periodontology, The Netherlands, 2004 (Published)

4. Yu, Wei-wen, and Roger A. LaBoube. *Cold-formed Steel Design*. New York: Wiley, 1985. Print.

5. Wang, C. M., C. M. Wang, C. Y. Wang, and J. N. Reddy. *Exact Solutions for Buckling of Structural Members*. Boca Raton, FL: CRC, 2004. Print.